Two-Dimensional Spectroscopy of Extended Molecular Systems

Dijkstra, Arend G.; Jansen, Thomas L. C.; Knoester, Jasper

Published in:
The Journal of Physical Chemistry A

DOI:
10.1021/jp9111124

Publication date:
2010

Two-Dimensional Spectroscopy of Extended Molecular Systems: Applications to Energy Transport and Relaxation in an α-Helix

Arend G. Dijkstra, Thomas L. C. Jansen, and Jasper Knoester*

Center for Theoretical Physics and Zernike Institute for Advanced Materials, University of Groningen, Nijenborgh 4, 9747 AG Groningen, The Netherlands

Received: November 23, 2009; Revised Manuscript Received: February 26, 2010

A simulation study of the coupled dynamics of amide I and amide II vibrations in an α-helix dissolved in water shows that two-dimensional (2D) infrared spectroscopy may be used to disentangle the energy transport along the helix through each of these modes from the energy relaxation between them. Time scales for both types of processes are obtained. Using polarization-dependent 2D spectroscopy is an important ingredient in the method we propose. The method may also be applied to other two-band systems, both in the infrared (collective vibrations) and the visible (excitons) parts of the spectrum.

I. Introduction

Nonlinear spectroscopy exploiting sequences of ultrashort pulses of visible or infrared radiation offers a rich tool box for unraveling the energetics and ultrafast dynamics of electronic and vibrational states of molecular systems. In particular, two-dimensional infrared (2DIR) and visible (2Dvis) spectroscopy[1] are rapidly gaining popularity to probe energy transport and relaxation in complex molecular systems. These spectroscopies have been developed during the past decade as analogues of two-dimensional NMR (2DNMR) experiments. In particular, the analogues of the NOESY variant of 2DNMR allow for the study of dynamics, because they involve a waiting time t_2 that may be controlled at the femtosecond time scales, thus allowing one to take snapshots of a system while it evolves.[2,3] Examples of systems that have been studied using 2DIR or 2Dvis spectroscopies with nonzero waiting times include relatively simple few-level systems, such as the coupled amide I and amide II vibrations in N-methylacetamide (NMA)[4] and vibrations in other small organic molecules,[5] as well as extended systems with a multitude of levels, such as the amide I band in polypeptides or proteins,[6,7] the excitonic transitions in the photosynthetic Fenna−Matthew−Olsen complex,[8] and the excitonic transitions in double-wall molecular nanotubes.[9]

In the simplest situation, with only two interacting vibrational or electronic states of interest, it is rather straightforward to obtain information about their coupled dynamics from the waiting time dependence of the 2D spectrum. In particular, the evolution of the diagonal peak of each state in this spectrum yields direct information on its lifetime (induced by decay to the other state or to a bath), while the cross peak between both states yields direct information on population transfer between them and possible coherence in the dynamics involved. More specifically, the waiting time dependence of the intensity of the cross peak normalized by the diagonal peak intensity is directly proportional to the population transfer, as has been shown for the amide I to amide II energy transfer in NMA.[10,11] For systems with a few, but more than two, states of interest, the dynamics may be deduced in a similar way.

The situation is less obvious for the coupled dynamics of two types of vibrations or electronic excitations in extended systems composed of many coupled building blocks. Such so-called two-band problems are ubiquitous in nature and in synthetic systems. Examples are the electronic energy transfer and relaxation in and between the B800 and the B850 rings of the light-harvesting antenna system in purple bacteria,[12–15] the dynamics of vibrational energy of the amide I and amide II vibrations in peptide helices, and electronic energy transfer in and between the inner and the outer cylinder in double-wall molecular nanotubes.[9] Each type of excitation in such extended systems gives rise to a band of collective excited states, which may be delocalized over many building blocks. As a result of (approximate) symmetry, usually only a few—so-called bright or superradiant—states dominate the optical (absorption) spectrum of each band; the many other states are dark, that is, they are not or are hardly visible in the spectrum. This makes a phenomenological interpretation of the associated 2D spectra in terms of only a few coupled states, derived from the bright states seen in the spectrum, very tempting. Yet, this simplicity is deceptive and leads to wrong results. The reason is that the many dark states still play a role in the dynamics and influence the 2D spectra. For instance, monitoring the intensity of the diagonal peak associated with a particular band of states, in contrast to a real few-level system, does not necessarily yield information about the energy loss from that band; the loss of intensity may also arise from transfer of energy from the superradiant states to the dark states within the same band. Disentangling intraband dynamics from interband dynamics and defining an operational way to measure the interband energy transfer rate is a hard problem.[16]

In this article we will show that using the combined information from several polarization dependent 2D spectra taken as a function of the waiting time, it is in fact possible to disentangle intraband and interband energy transport and relaxation, and to obtain the separate time scales for these types of dynamics from experiment. We will do this by simulating the coupled dynamics of the amide I and amide II vibrations in model α-helices dissolved in water (see Figure 1) and calculating the 2DIR spectra as a function of t_2. Aside from the generic interest in this type of two-band problems, the topic of vibrational energy transport within peptide helices is one that

* To whom correspondence should be addressed. E-mail: j.knoester@rug.nl.

10.1021/jp9111124
Published on Web 05/28/2010

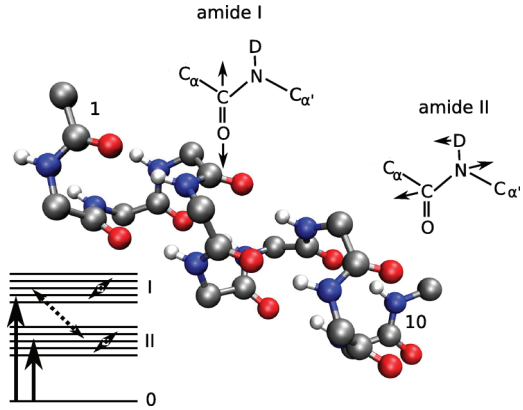

Figure 1. The α-helix consisting of 10 amide groups, numbered 1 through 10 from the N to the C terminus. In the structure formulas, the distortion along the amide I and amide II normal mode coordinates is indicated with arrows. To the lower left, the energy level diagram is depicted schematically, with the ground state (0), the band of 10 collective vibrations of amide II character (II) and the band of 10 collective amide I vibrations (I). The thick arrows starting from the ground state symbolize the excitation processes, and the double-sided arrows symbolize the intraband (solid) and interband (dashed) relaxation processes.

has intrigued researchers for several decades already.[17] The development of 2DIR spectroscopy has recently given new impetus to this area.[7,18]

II. Modeling Vibrational Energy Transport

The model for the α-helix and the nature of the amide I and amide II vibrations that occur within each amide group are schematically depicted in Figure 1. The results reported were obtained for a helix of 10 amide groups, implying that 20 local amide vibrations were taken into account. We did examine systems of different size and found that a length of 10 amide groups is sufficient to exclude finite-size effects. The amide I vibration has a strong infrared response, making it the most frequently probed vibration in polypeptides. As a second mode we consider amide II, because its spatial and energetic proximity to amide I give rise to quite fast relaxation between them,[10] facilitated by a resonance that includes the solvent. In the helix, the electrodynamic and mechanical couplings between local vibrations give rise to amide I and amide II bands of collective vibrations, as is also depicted in Figure 1. Fluctuations in the surrounding solvent now result in transport and relaxation within each band as well as relaxation between both bands. The excited amide modes can also transfer their energy to multiple quanta of low-frequency vibrations in the peptide, as seen in studies[5] on organic systems. Recent quantum chemical calculations suggest that the role of these states is not of prime importance in our system.[11] Including such states, for which little is known in our system, would be prohibitively expensive computationally, and this type of dark states are therefore neglected.

Within the model, each amide group may carry a vibrational energy quantum in each of the two modes considered; the natural frequencies of these local modes are on the order of 1600 cm^{-1} for amide I and 1500 cm^{-1} for amide II. The one-quantum excitations of these two modes form the basis for describing the vibrational energy transport. To model the nonlinear response probed in the 2DIR spectrum, the amide I and amide II overtones on each amide group are also considered, as well as the combination state in which both modes carry one vibrational quantum.

Including the coupling between the local vibrations, this leads to the Hamiltonian for the relevant states:

$$H = \hbar \sum_{n,i} \left[\omega_{ni} a_{ni}^{\dagger} a_{ni} - \frac{A_i}{2} a_{ni}^{\dagger} a_{ni}^{\dagger} a_{ni} a_{ni} \right] + \hbar \sum_{n,i,m,j} J_{ni,mj} a_{ni}^{\dagger} a_{mj} \quad (1)$$

Here, n and m label the amide units (so, they both run from 1 to 10 in our case), while i and j can be either 1 (for the amide I vibration) or 2 (amide II). The operators $a_{ni}^{\dagger}$ and a_{ni} are the usual ladder operators for harmonic oscillators. The first term describes the energy of a single amide unit, accounting for the natural frequency ω_{ni} of each of the oscillators as well as for the anharmonic frequency shift A_i of the overtones.

The second term describes the bilinear interaction between the different local oscillators, characterized by the $J_{ni,mj}$. Values for these parameters are obtained from the electrodynamic transition charge coupling (TCC) model.[19,20] Because mechanical coupling is important between amide units that are connected through covalent bonds, the TCC model can not be applied there. Instead, we have created a nearest-neighbor coupling map for the amide I and II modes from DFT calculations on a dipeptide using the matrix reconstruction method. The procedure is an extension to the one applied previously for the amide I band in polypeptides.[20–25] The reconstruction method also produces values for shifts in the harmonic frequency of the oscillators due to the peptide environment, which are included in the parameters ω_{ni}. For the anharmonic shifts we accepted the values deduced from experiments on NMA (16 cm^{-1} for amide I (ref 6) and 11 cm^{-1} for amide II (ref 4)).

Due to the interactions $J_{ni,mi}$ partially delocalized vibrational states arise in both amide bands.[26,27] In each band the spectrum is dominated by the bright so-called A and E modes. For the A modes, the amide oscillations on different groups occur in phase; the A mode has a transition dipole oriented parallel to the axis of the helix. The E modes occur where the phase relation between the local vibrations result in transition dipoles perpendicular to the helical axis. For amide I the A mode is much brighter than the E modes, whereas the opposite is true for amide II. As the energy difference between the A and E modes is on the order of 10 cm^{-1} for amide I[27] and even smaller for amide II,[28] it is in practice very hard to distinguish these modes under the broad line shape that occurs for helices in typical environments. Thus, the infrared spectrum of the α-helix is dominated by one bright peak associated with each one of the bands considered, making it appear as a two-state system. It should be realized that in addition to the fact that more than one state underlies each spectral peak, even more dark states occur in each band (7 for the case of a length-10 helix), all of which affect the vibrational dynamics.

To describe (incoherent) energy transport and relaxation, the effects of the solvent on the amide vibrations are crucial. The configuration of water molecules in the environment of the α-helix is fluctuating on ultrashort time scales (down to 100 fs), as seen in other peptide systems.[3,18] The partial charges in these molecules affect the vibrations through Stark shifts,[29,30] which constantly change in time, due to the solvent dynamics. As a result, the Hamiltonian in eq 1 is time dependent, of the so-called fluctuation oscillator form.[1] In our simulations we have included fluctuations of the local amide I and amide II frequencies as well as the solvent induced coupling $J_{n1,n2}$ between them. This is done by combining molecular dynamics

simulations of an NMA-d_7 molecule (a single amide unit) in water with a DFT map that translates the local water configuration into frequency shifts. This leads to autocorrelation and cross-correlation functions for the local frequencies and the coupling on each amide unit, from which trajectories for the time-dependent Hamiltonian are derived. In this procedure, the fluctuations must be Gaussian. From looking at three- and four-point correlation functions, we conclude that this is indeed a good approximation in our MD results, as was the case in NMA-d.[10] The couplings between different groups are assumed to be constant, because, typically, their fluctuations are found to be much smaller than fluctuations in the oscillator frequencies. From MD simulations of trialanine, coupling fluctuations of a few wavenumbers were found,[25] and we expect these fluctuations to be smaller in the more rigid helix. Furthermore, although the fluctuating quantities within an amide group are correlated, we do not include correlations between different groups. This approach allows us to parametrize the time dependence of the Hamiltonian from simulations of a single peptide group. We also excluded possible fluctuations in the anharmonicity. The effect of such fluctuations on the spectra of the amide I mode is known to be small.[29]

Other parameters that we need in the calculation of the spectra are the average energy gap between the two modes and the average transition dipoles. The energy gap includes shifts from the dipeptide map, and is 137.2 cm^{-1}, and the average on-site coupling between both modes is 44.4 cm^{-1}. From the average over the MD trajectory, the angle between the amide I and amide II transition dipoles is 79.4°, which compares well to the 75° found experimentally in ref 4; and the length of the amide II dipole is 0.64 times the length of the amide I dipole (compared to a value extracted from experiments of 0.58). Fluctuations in the dipoles have been neglected.

The fast fluctuations nonadiabatically mix all states on a short time scale, rendering the picture of static eigenstates, although useful for an understanding of the spectrum, invalid for a proper description of the vibrational dynamics. We have therefore computed the dynamics generated by the time-dependent Hamiltonian by numerically integrating the time-dependent Schrödinger equation.[31] From this the wave function at each moment in time may be obtained following some initial excitation condition. This gives information on the time dependence of the excitation probabilities of different vibrations in the system and the phase relations between them. In particular, this allows one to calculate the probability that after some time t an initial excitation still resides in the band in which it was created initially, as well as the velocity of energy propagation or the diffusion constant within a band. Using the numerical integration of the Schrödinger equation, we fully include nonadiabatic vibrational dynamics in the amide I and II bands. The only approximation comes from neglecting the effect of these vibrations on the environment, which leads to a high-temperature description.

Finally, the numerical integration of the Schrödinger equation also allows one to calculate the linear and 2D absorption spectra through standard perturbation theory in the infrared or visible laser fields.[31,32] These calculations allow us to connect the information about the energy transport mechanisms described in the previous paragraph with quantities that are observable in experiment. The most time-consuming step in the calculation is the propagation of the two-quantum states needed in the nonlinear optical response. To simplify this, we use the Trotter factorization to separate the harmonic and anharmonic contributions in each time step. The anharmonic contribution can be calculated fast, while the harmonic propagator is simply given as the product of one-exciton propagators.[33]

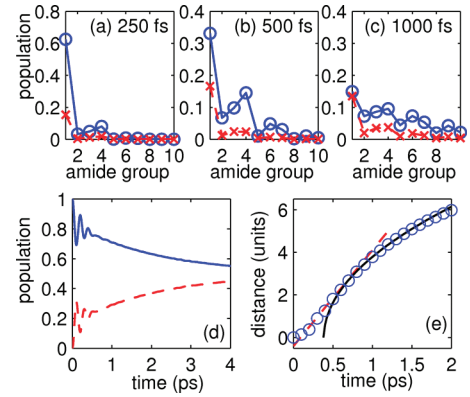

Figure 2. (a−c) Amide I (circles) and amide II (crosses) populations in a length 20 α-helix at various waiting times after initial excitation of the amide I oscillator on group 1. The amide groups are indexed from the N to the C terminus. (d) Total population in the amide I band (solid line) and the amide II band (dashed line) after initial excitation of this mode. (e) The average distance traveled by an amide I excitation in an α-helix after initial excitation of this mode on the first amide group from the N terminus. The open circles are the result of our calculation. A ballistic fit at short times and a diffusive fit at longer times are indicated by a dashed and a solid line, respectively.

Results and Discussion

A. Transport and Relaxation. The transport of vibrational energy within a particular amide band and the relaxation between both bands may be characterized by solving for the vibrational wave function as a function of time following the initial one-quantum excitation of one of the oscillators in one of the bands. Figure 2a−c shows the time evolution of the vibrational wave packet after exciting at time zero the first amide I oscillator counted from the N terminus of the helix. Circles show the probability that the amide I vibration on a certain site is excited, while crosses show these probabilities for the amide II vibrations. These figures clearly demonstrate that population transport within the amide I band and relaxation between both bands take place on time scales of the order of 1 ps or less.

As is observed, the transport within the amide I band occurs most efficiently between hydrogen bonded amide groups, such as the first one and the fourth. The reason is that the coupling between the dipoles of such groups is large, as a result of the alignment of their transition dipoles. However, as is seen from Figure 2b, transport also occurs between nearest neighbors along the backbone of the helix, albeit slower: the increase in the population on site 2 is clearly smaller than the growth of the population on site 4.

To describe the intraband and interband dynamics in a more quantitative way, we have integrated the information from the wave packets in two different ways. First, Figure 2d displays the time evolution of the total populations in the amide I and amide II bands of the helix as a function of time. During the first few hundred femtoseconds, small oscillations take place caused by population coherently transferring back and forth between both bands. The period of the oscillations is 0.2 ps, corresponding to a linear frequency of $\omega/2\pi c = 165$ cm^{-1}, which is equal to the energy gap between the amide I and amide II band. At longer waiting times the decay of the total amide I population is exponential with a lifetime of 2.12 ± 0.01 ps. We take this number as the time scale for the interband relaxation. Second, Figure 2e shows the distance d traveled in

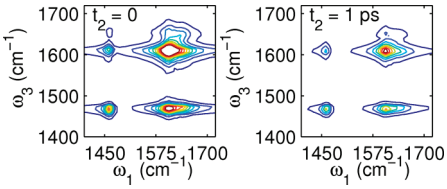

Figure 3. Absolute value rephasing 2DIR spectrum (parallel polarization) of a length 10 α-helix for waiting time (t_2) zero and 1 ps. Contours are drawn between 5 and 50% of the maximum intensity in the left panel, at intervals of 5%.

the amide I band, defined using the quantum mechanical expectation value of the position operator. In the first 700 fs, the distance can be fitted with a straight line ($d = t/0.22$ ps -0.4). This can be interpreted as ballistic transport with a rate of about 4 peptide units per ps, arising as a consequence of the partial delocalization. Here, the offset -0.4 reflects the nonlinear behavior of d with t at early times, which is a consequence of the initial accelerated vibron motion. After approximately 700 fs, the excitation transport can be characterized as diffusive due to the finite scattering length, with a one-dimensional diffusion constant D (here defined by $d^2 = 2Dt$) of 11 peptide units squared per picosecond. Similarly, the ballistic dynamics in the amide II band—measured after exciting the amide II oscillator at site 1—takes place with a time constant of 0.9 ps ($d = t/0.94$ ps $- 0.4$) for about 4 ps, after which diffusive motion sets in with the diffusion constant of 4 peptide units squared per picosecond. From our simulations we can characterize both the intra- and interband dynamics. As was mentioned in the introduction, this is, however, not straightforward in an experiment.

B. 2DIR Spectra. Detailed information on the dynamics is present in a 2D spectrum. This displays the third-order optical signal collected in an experiment exploiting four infrared or visible laser pulses with variable delays times between them.[1] To probe the vibrational or electronic dynamics, the delay time between the first and the second pulse pair is particularly important; this is usually referred to as the waiting time. The signal measured is complex valued, and multiple ways of plotting it have been devised. Here, we will only use the absolute value of the signal. In an approximate, but useful, picture, the spectrum can be interpreted as the correlation between the state of the system before and after the waiting time. The transition frequency of the former state (prepared by the first pulse pair) is denoted ω_1 and is plotted on the horizontal axis of a 2D map, as is shown in Figure 3; the frequency of the latter state, probed by the second pulse pair, is denoted ω_3 and is displayed along the vertical axis. For the example of the α-helix, the most intense peaks in the spectra are found on the vertical line with ω_1 around 1600 cm^{-1}. They both correspond to initial excitation of the amide I mode. The strongest of these peaks, found on the $\omega_1 = \omega_3$ diagonal, is a result of pathways where the system is still in an amide I state after the waiting time, while the lower peak (cross peak) contains information about the coupling to the amide II band.

Apart from the all-parallel polarization, resulting in the spectra shown in Figure 3, the two laser pulses arriving after the waiting time may also be chosen with a polarization perpendicular to that of the two pulses arriving before the waiting time. The difference between the integrated peak intensities in the parallel and perpendicular absolute value spectra, normalized to the isotropic signal, is a measure of the anisotropy of the excited vibrational state.[6] In systems where not all dipoles have the same orientation (such as the α-helix), the anisotropy will decay over

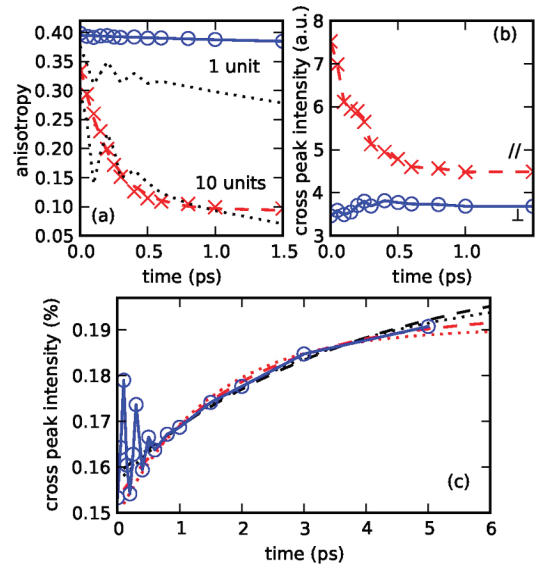

Figure 4. (a) Polarization anisotropy of the integrated amide I diagonal peak intensities (rephasing spectrum) with exponential fit for a length 10 helix (crosses) and for a single amide unit (circles). Also shown are the calculation results for the amide II diagonal peak (dotted lines). (b) Integrated intensities of the upper amide II−amide I cross peak in a length 10 helix (non-rephasing spectrum) for parallel (crosses) and perpendicular (circles) polarization arrangement of the laser pulses. (c) Integrated intensity of the upper cross peak in the absolute value non-rephasing 2DIR spectrum (parallel polarization) of a length 10 α-helix, normalized to the total integrated intensity in the spectrum. Also shown in panel (c) are exponential fits to the calculated points between 600 and 5000 fs, with time constants 1.5 ps (dotted red), 2 ps (dashed red), 3 ps (dotted black), and 4 ps (dashed black).

time, reflecting the transport of vibrational energy from the originally excited states to others, with different polarization.

Thus, the evolution of the anisotropy of the amide I diagonal peak with the waiting time should contain information about the transport of vibrational energy through the amide I band. Figure 4a (crosses) shows this anisotropy, revealing a decay on a sub-picoseconds time scale. This is considerably faster than the anisotropy decay within a single amide unit (which is plotted as squares in the same panel); for a single unit the decay cannot reflect transport, but solely results from fluctuation-induced mixing of the amide I and amide II modes as time progresses. Thus, Figure 4a is consistent with the idea that fast transport over the helix is responsible for reducing the anisotropy. A more quantitative analysis confirms this explanation. We first consider the initial value of the anisotropy. In an eigenstate picture, the initial excitation will mainly populate the intense A mode of the helix, where all amide I vibrators move in phase.[27,34] In an isotropic solution of helices, the polarization anisotropy should then be 0.4 at zero waiting time. Its somewhat smaller value in our results of Figure 4a can be explained from the nature of the amide I diagonal peak, which does not originate from a single transition, but contains contributions from an A−E cross peak as well.[27]

At longer waiting times, as a result of the fluctuations, the initially excited state relaxes, that is, it transfers its energy to other states within the amide I band. Thus, the average dipole of the excitation is rotated, which leads to the observed decay of the anisotropy. Over the entire time interval shown, the decay is fitted very well by an exponential function, with a decay time of 0.23 ± 0.04 ps. This time scale agrees nicely with the ballistic transport time in the amide I band found above. The longer diffusive time is not observed, because the memory of the

polarization direction is already lost during the ballistic period, where the excitation moves a few units. We found that also the amide II diagonal peak complies with this picture. Although the oscillations in the first 400 fs (see Figure 4) complicate the analysis, they are followed by an exponential decay with a decay time of 0.8 ± 0.1 ps, which again agrees well with the ballistic transport time for this mode.

The intraband dynamics, thus, shows up in the polarization anisotropy of the diagonal peaks. We now turn our attention to the amide II−amide I cross peaks. We focus on the one found in the upper left corner of the non-rephasing spectrum. The other cross peak essentially contains the same information. Because the cross peak results from the interaction between the amide I and II bands, it is expected to contain information about the interband relaxation. To see that the collective nature of the amide modes is also important here, we will first analyze our results with an oversimplified model. In view of the simple structure of the spectrum, it is tempting to treat each of the bands as a single, effective mode. The 2DIR spectrum calculated from such a model would contain diagonal amide I and II peaks, as well as amide I−amide II cross peaks. Although these main features of the 2DIR spectrum are reproduced, the simple model is not able to explain the variation in the cross peak intensity that we observe in the full calculation. The cross peaks between the amide I and amide II modes would be expected to increase in intensity with waiting time as a result of the vibrational relaxation between these two modes.[10] However, as we have seen in the polarization anisotropy, the intraband relaxation leads to rotation of the dipole of the excitation in our full model. In combination with the relaxation to dark states within the same exciton band, this leads to a *decrease* in the cross peak intensity in the parallel polarization in the first 600 fs (Figure 4b, crosses). It is clear that the intraband dynamics, which is neglected in the simple model, needs to be included properly to be able to fully understand the time evolution of a cross peak in the 2DIR spectrum. For the perpendicular polarization a small initial rise is observed. In this case the rotation of the dipole increases the peak intensity (Figure 4b, circles).

The question then arises of how the cross peak intensity may be corrected for the effect of intraband dynamics, so that it only reflects the interband relaxation, thus allowing for a method to extract the corresponding time scale from experiment. Because all contributions to the spectrum depend on the intraband dynamics, and assuming that the dynamics is essentially the same in different parts of the spectrum, the cross peak intensity normalized to the total intensity in the spectrum should be determined mainly by the interband dynamics. This quantity is plotted as a function of waiting time in Figure 4c. After initial oscillations, corresponding to those observed in the total populations of Figure 2, the normalized cross peak intensity does increase. The limited dynamic range in Figure 4 makes it hard to find a unique fit to the intensity increase. Shown are exponential fits with growth times between 1.5 and 4 ps; the best fit is obtained with a time scale of 2 ps, which indeed corresponds to the interband relaxation time found earlier. Although the assumption that the intraband dynamics is the same for both modes contrasts with the different values found for the ballistic time scales, it is supported by the anisotropy data presented in Figure 4a. Furthermore, the largest effect on the cross peak intensity originates in the fastest intraband dynamics. For our system, this is the dynamics in the amide I band, which also contributes most to the total intensity in the spectrum because of the large amide I transition dipole. In a system where the fastest intraband relaxation is found for the mode with the lowest oscillator strength, additional normalization procedures might be devised. Nevertheless, our calculation demonstrates that the normalization procedure presented here correctly accounts for the effects of intraband dynamics in the cross peak.

In the present report we have looked at the possibility to characterize transport in the unmodified system. An alternative is to change selected sites by using isotope labeling or chemical modification[7] and then monitoring the transport between these selected sites. Although this method will possibly allow the observation of the diffusive time scale, it has the disadvantage that the transport between a modified site and the band formed by the other sites will be altered and this has to be accounted for. In the approach presented above the observed transport is intrinsic to the system.

IV. Conclusion

In this paper we demonstrated how 2D spectroscopy may be used to disentangle the intraband and the interband relaxation in systems with two coupled bands of collective excited states. As a special example we have studied the coupled dynamics of the amide I and II bands in a model α-helix dissolved in water. We have shown that, in contrast to a real two-state system, the waiting time dependencies of the intensities of the two diagonal and two cross peaks that dominate the 2D spectrum of the helix do not directly yield the intraband and interband relaxation rates. The reason is that the relaxation to dark states influences the intensities as well. We found that measuring the polarization anisotropy of the diagonal peaks and normalizing the cross peaks to the total intensity in the spectrum, allows one to account for the dark states, that is, for the collective nature of the excitations in the two bands.

Within our model we could distinguish ballistic and diffusive intraband transport in both bands. The time scales for the ballistic transport (characterized by the time it takes to move to a nearest-neighbor amide unit) were found to be 0.2 and 0.9 ps for amide I and amide II, respectively. Diffusive motion sets in after about 0.7 and 4 ps for the amide I and amide II bands, respectively, with diffusion constants given by 11 and 4 units^2/ps. Finally the interband relaxation time constant was found to be 2.1 ps. The latter is considerably slower than the 790 fs found for NMA-*d* with a similar simulation method;[35] this difference results from the fact that the energy gap between the amide I and the amide II bands is larger than the energy difference between both vibrations in NMA-*d*. This is consistent with the experimental observation that the relaxation from the amide I mode in proteins is slower than in NMA-*d*.[6] Although we believe that solvent-assisted mixing with the amide II mode forms a prime channel for the relaxation of the amide I mode, other relaxation channels will contribute as well.[36] On longer time scales the energy will completely disappear from the amide I and amide II bands. Including all possible accepting modes is prohibitively expensive computationally at the moment and their treatment is a challenge for the further development of the method presented here.

Since in the parametrization of our model we used the fluctuations of the vibrational constants in NMA-d_7 in heavy water, we probably overestimated the importance of the fast water dynamics: the surrounding of the amide groups in a helix is somewhat less dominated by water than in a single NMA-d_7 molecule. In addition, our approach neglects the role of slow conformational changes in the helix; at least for short helices such changes have been seen.[27] Finally, the real fluctuations will also depend on the helix environment (membrane, free-floating, or muscle fiber). Thus, in practice the dynamics may

be different (slower) from that predicted by our model calculation. However, this does not affect our most important result, namely that intra- and interband dynamics may be characterized using 2D spectroscopy. We believe that this general result will also be of use for other extended systems with bands of collective excitations, provided that the dipoles in the system vary in direction, so that transport is reflected in the polarization of the excitation.

Acknowledgment. T.L.C.J. acknowledges The Netherlands Organization for Scientific Research (NWO) for support through a VIDI grant.

References and Notes

(1) Cho, M. *Chem. Rev.* **2008**, *108*, 1331–1418.
(2) Zanni, M. T.; Gnanakaran, S.; Stenger, J.; Hochstrasser, R. M. *J. Phys. Chem. B* **2001**, *105*, 6520–6535.
(3) Jansen, T. l. C.; Knoester, J. *Biophys. J.* **2008**, *94*, 1818–1825.
(4) DeFlores, L. P.; Ganim, Z.; Ackley, S. F.; Chung, H. S.; Tokmakoff, A. *J. Phys. Chem. B* **2006**, *110*, 18973–18980.
(5) Kurochkin, D. V.; Naraharisetty, S. R. G.; Rubtsov, I. V. *Proc. Natl. Acad. Sc. USA* **2007**, *104*, 14209–14214.
(6) Hamm, P.; Lim, M.; Hochstrasser, R. M. *J. Phys. Chem. B* **1998**, *102*, 6123–6138.
(7) Botan, V.; Backus, E. H. G.; Pfister, R.; Moretto, A.; Crisma, M.; Toniolo, C.; Hamm, P. *Proc. Natl. Acad. Sc. USA* **2007**, *104*, 12749–12754.
(8) Brixner, T.; Stenger, J.; Vaswani, H. M.; Cho, M.; Blankenship, R. E.; Fleming, G. R. *Nature* **2005**, *434*, 625–628.
(9) Nemeth, A.; Milota, F.; Sperling, J.; Abramavicius, D.; Mukamel, S.; Kauffmann, H. F. *Chem. Phys. Lett.* **2009**, *469*, 130–134.
(10) Dijkstra, A. G.; Jansen, T. l. C.; Bloem, R.; Knoester, J. *J. Chem. Phys.* **2007**, *127*, 194505.
(11) Zhang, Y.; Fujisaki, H.; Straub, J. E. *J. Phys. Chem. A* **2009**, *113*, 3051–3060.
(12) Zigmantas, D.; Read, E. L.; Mancal, T.; Brixner, T.; Gardiner, A. T.; Cogdell, R. J.; Fleming, G. R. *Proc. Natl. Acad. Sc. USA* **2006**, *103*, 12672.
(13) Cheng, Y. C.; Silbey, R. J. *Phys. Rev. Lett.* **2006**, *96*, 028103.
(14) Sundström, V.; Pullerits, T.; van Grondelle, R. *J. Phys. Chem. B* **1999**, *103*, 2327–2346.
(15) Xu, X. C.; Schulten, K. *Phys. Today* **1997**, *50*, 28–34.
(16) Didraga, C.; Malyshev, V. A.; Knoester, J. *J. Phys. Chem. B* **2006**, *110*, 18818–18827.
(17) Davydov, A. S. *Solitons in Molecular Systems*; Reidel: Dordrecht, 1985.
(18) Backus, E. H. G.; Nguyen, P. H.; Botan, V.; Pfister, R.; Moretto, A.; Crisma, M.; Toniolo, C.; Stock, G.; Hamm, P. *J. Phys. Chem. B* **2008**, *112*, 9091–9099.
(19) Hamm, P.; Woutersen, S. *Bull. Chem. Soc. Jpn.* **2002**, *75*, 985–988.
(20) Jansen, T. l. C.; Dijkstra, A. G.; Watson, T. M.; Hirst, J. D.; Knoester, J. *J. Chem. Phys.* **2006**, *125*, 044312.
(21) Torii, H.; Tasumi, M. *J. Raman Spectrosc.* **1998**, *29*, 81–86.
(22) Ham, S.; Kim, J. H.; Lee, H.; Cho, M. *J. Chem. Phys.* **2003**, *118*, 3491–3498.
(23) Schmidt, J. R.; Corcelli, S. A.; Skinner, J. L. *J. Chem. Phys.* **2004**, *121*, 8887–8896.
(24) Hayashi, T.; Zhuang, W.; Mukamel, S. *J. Phys. Chem. A* **2005**, *109*, 9747–9759.
(25) Gorbunov, R. D.; Kosov, D. S.; Stock, G. *J. Chem. Phys.* **2005**, *122*, 224904.
(26) Miyazawa, T. *J. Chem. Phys.* **1960**, *32*, 1647–1652.
(27) Woutersen, S.; Hamm, P. *J. Chem. Phys.* **2001**, *115*, 7737–7743.
(28) DeFlores, L. P.; Ganim, Z.; Nicodemus, R. A.; Tokmakoff, A. *J. Am. Chem. Soc.* **2009**, *131*, 3385–3391.
(29) Jansen, T. l. C.; Knoester, J. *J. Chem. Phys.* **2006**, *124*, 044502.
(30) Fecko, C. J.; Eaves, J. D.; Loparo, J. J.; Tokmakoff, A.; Geissler, P. L. *Science* **2003**, *301*, 1698–1702.
(31) Jansen, T. l. C.; Knoester, J. *J. Phys. Chem. B* **2006**, *110*, 22910–22916.
(32) Mukamel, S. *Principles of Nonlinear Optical Spectroscopy*; Oxford University Press: Oxford, 1995.
(33) Paarmann, A.; Hayashi, T.; Mukamel, S.; Miller, R. J. D. *J. Chem. Phys.* **2009**, *130*, 204110.
(34) Ham, S.; Hahn, S.; Lee, C.; Kim, T.; Kwak, K.; Cho, M. *J. Phys. Chem. B* **2004**, *108*, 9333–9345.
(35) Bloem, R.; Dijkstra, A. G.; Jansen, T. l. C.; Knoester, J. *J. Chem. Phys.* **2008**, *129*, 055101.
(36) Fujisaki, H.; Stock, G. *J. Chem. Phys.* **2008**, *129*, 134110.

JP9111124